energies

MDPI

Article

Free Convective Heat Transfer in a Closed Gap between Concentric Semi-Hemispheres

Abderrahmane Baïri [1,*], Nacim Alilat [1], Alexander Martín-Garín [2], Kemi Adeyeye [3], José-Antonio Millán-García [2] and Luis Roseiro [4]

[1] Laboratoire Thermique Interfaces Environnement (LTIE), Université de Paris, EA 4415, 50 Rue de Sèvres, F-92410 Ville d'Avray, France; nacim.alilat@gmail.com
[2] ENEDI Research Group, Department of Thermal Engineering, Faculty of Engineering of Gipuzkoa, Universidad del Pais Vasco UPV/EHU, Plaza Europa 1, 20018 Donostia-San Sebastián, Spain; alexander.martin@ehu.eus (A.M.-G.); j.millan@ehu.eus (J.-A.M.-G.)
[3] Department of Architecture and Civil Engineering, University of Bath, Bath BA2 7AY, UK; ka534@bath.ac.uk
[4] Polytechnic of Coimbra, ISEC, Rua Pedro Nunes—Quinta da Nora, 3030-199 Coimbra, Portugal; lroseiro@isec.pt
* Correspondence: abairi@u-paris10.fr

Abstract: Free convective heat transfer in the closed gap between concentric semi-hemispheres is quantified by means of a numerical approach based on the volume control method using the SIMPLE algorithm. The average Nusselt number is determined for several configurations obtained by varying the cavity's aspect ratio between 0.15 and 1.5, while the Rayleigh number varies within the 5.33×10^3–4.50×10^8 range. The results show that the correlations available in the literature dealing with concentric whole spheres cannot be used for the configuration treated here. The new correlation between the Nusselt and Rayleigh numbers proposed in this work can be applied in various engineering sectors, such as in the electronic packaging considered in this present work, buildings, and architecture.

Keywords: natural convection; electronic packaging; numerical approach; concentric semi-hemispheres; buildings; architecture

Citation: Baïri, A.; Alilat, N.; Martín-Garín, A.; Adeyeye, K.; Millán-García, J.-A.; Roseiro, L. Free Convective Heat Transfer in a Closed Gap between Concentric Semi-Hemispheres. *Energies* **2021**, *14*, 7479. https://doi.org/10.3390/en14227479

Academic Editor: Dmitry Eskin

Received: 30 August 2021
Accepted: 19 October 2021
Published: 9 November 2021

1. Introduction

Several works dealing with quantification of heat transfer by free convection have been carried out in both variable regime and steady state. Different fluids and flow regimes have been examined for cavities or spaces of various shapes [1–6]. The hemispherical geometry has been treated recently with experimental and numerical approaches, applied to some engineering fields, such as buildings and renewable energy. The influence of various physical parameters on heat transfer are examined, such as thermal conditions, thermophysical characteristics of the considered fluid, Rayleigh number range, and the enclosure's inclination angle with respect to the gravity's direction. Heat transfer by natural convection occurring in these enclosures was quantified in [7] at steady state through Nusselt–Rayleigh type correlations. A non-exhaustive synthesis of these correlations was presented in [8] for air-filled hemispherical cavities under various geometrical and thermal boundary conditions. Heat transfer for high heat flux generation systems using various nanofluids have also been quantified in some experimental and numerical studies, such as [9–12]. The study [13] quantifies the free convective heat transfer between inclined concentric hemispheres, separated by different nanofluids whose volume fraction varies in different ranges depending on the concerned engineering application. The study [14] deals with free convection via porous media saturated by nanofluid in annular spaces. The proposed correlations allow determination of the average Nusselt number for various combinations of some influencing physical parameters. Unsteady free convective

phenomena between whole concentric spheres have been examined in [15] through a mathematical modeling. The presented temperature and velocity fields highlight the influence of some physical parameters, such as the energy source on the flow structure and heat exchange. The dynamic and thermal steady state phenomena have been determined for whole concentric spheres, and heat transfer was quantified via Nusselt–Rayleigh type correlations in several studies, such as [16–20]. The recent work [21] examines the case of an open air-filled enclosure consisting of two differentially heated semi-hemispheres, applied to the building field as is the case in [22]. Many combinations of the cavity's aspect ratio varying in the 0.05–3.5 range and Rayleigh number ranging between 9.22×10^7 and 6.76×10^{11} were considered. A correlation is proposed, allowing determination of the average Nusselt number.

The present work deals with quantification of heat transfer by free convection in a semi-hemispherical closed cavity. This configuration has been processed at the request of the electronics packaging sector for applications by means of this closed air-filled enclosure whose aspect ratio varies in the 0.15–1.5 range and Rayleigh number ranging between 5.33×10^3 and 4.50×10^8. This work completes the recent study [23] dealing with the thermal state of the cavity. A correlation is proposed there, allowing the determination of the average temperature difference between the walls of the cavity for any combination of the aspect ratio varying in the 0.05–0.35 range and the Rayleigh number ranging between 9.22×10^7 and 6.76×10^{11}.

2. The Treated Assembly

The work quantifies the free convective heat transfer between the concentric semi-hemispheres presented schematically in Figure 1.

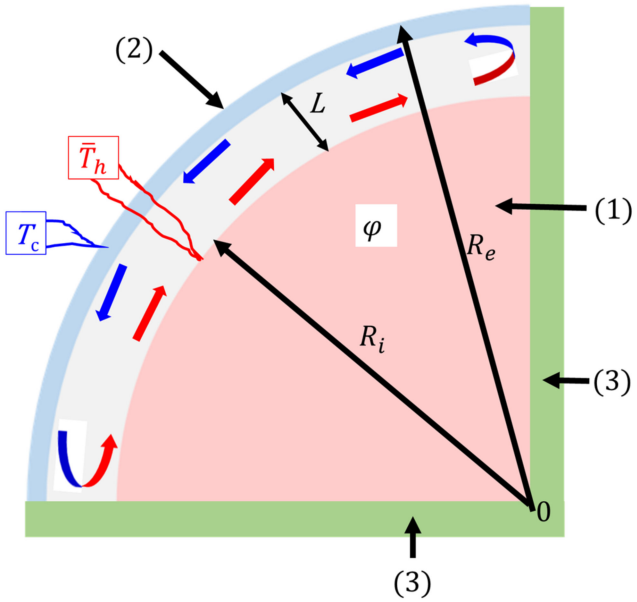

Figure 1. Scheme of the considered assembly.

The internal quarter sphere (1) of radius R_i generates a heat flux φ assumed to be constant. This active part constitutes the active electronic assembly cooled by natural air convection. Unlike the configuration discussed in [21], this assembly constitutes the entire quarter-sphere. Its average temperature reached during operation at steady state is denoted as $\overline{T}_h$. The outer wall (2) of radius R_e is isothermal, maintained at a temperature T_c. The back and lateral faces of the closed enclosure are thermally insulated (3). Distance L between the hot and cold walls (air layer) varies according to the considered enclosure's aspect ratio:

$$A = L/R_i \quad (1)$$

which takes seven values in this work: A = 0.15, 0.30, 0.50, 0.75, 1.00, 1.25, and 1.5. The overall walls' infra-red emissivity is assumed to be zero, the essential objective of this work being to determine the natural convective heat exchanges. This assumption eliminates calculation of radiative heat transfer, simplifies the calculation process and allows the free convective heat transfer to be determined with better precision.

3. Numerical Resolution

The considered problem is governed by the following dimensionless continuity, momentum, and energy equations, detailed in [20,21,24]:

$$\begin{gathered} \vec{\nabla}^{*}\vec{u}^{*} = 0 \\ \left(\vec{u}^{*}\vec{\nabla}^{*}\right)\vec{u}^{*} = -\vec{\nabla}^{*}p^{*} + Pr\nabla^{*2}\vec{u}^{*} + RaPrT^{*}\vec{e}_{g} \\ \left(\vec{u}^{*}\vec{\nabla}^{*}\right)T^{*} = \nabla^{*2}T^{*} \end{gathered} \tag{2}$$

In these equations, $\vec{\nabla}^{*}$ is the nabla operator, $\vec{e}_{g}$ is the unit vector opposite to the gravity field, while ∇^{*2} is the spherical Laplacian operator. The Prandtl number Pr, as well as dimensionless pressure p^{*}, temperature T^{*}, and velocity vector $\vec{u}^{*}$ are defined with:

$$Pr = \frac{\mu C_p}{\lambda};\ p^{*} = \frac{pL^2}{a^2\rho};\ T^{*} = \frac{T - T_c}{\frac{\varphi L}{\lambda}};\ \vec{u}^{*} = \frac{\vec{u}L}{a} \tag{3}$$

whereby, ρ, C_p, and $a = \lambda/\rho C_p$ are the air density, specific heat at constant pressure, and thermal diffusivity, respectively. The Rayleigh number Ra_L is based on the generated heat flux φ and air layer thickness L:

$$Ra_L = \frac{g\beta L^4\rho}{\mu\lambda a}\varphi \tag{4}$$

Thermophysical characteristics are calculated at the mean temperature $\left(\overline{T}_h + T_c\right)/2$. The governing system in Equation (2) is solved with a homemade software using the control volume method based on the well-known SIMPLE algorithm [24]. At the beginning of the process calculation, thermal gradient is assumed to be null on the internal face of the active wall, as well as on the lower face of the enclosure. Air is immobile, and the entire computational domain is isothermal at temperature T_c. During the process calculation, components of the velocity are zero over the walls of the enclosure. A heat balance is carried out at the air–wall interface to control the continuity of temperature and heat flux. The adopted mesh presented in Figure 2 is thus structured. A linear refinement is carried out in the air layers adjacent to the hot and cold walls of the enclosure. This allows the thermal gradients to be determined with higher accuracy. This operation is important for determining convective exchanges, the main objective of this study. The starting version of the mesh consists of 230,000 elements. The process adopted for its optimization consisted of increasing it in steps of 5%. This operation is carried out until the mean Nusselt number no longer varies by more than 2%. This occurred after consecutively increasing the number of elements three times. This condition is associated with the convergence criteria of 10^{-3}, 10^{-6}, and 10^{-5} for the continuity, energy, and momentum equations, respectively. With this numerical approach, the mesh-independent solution with 383,259 elements is finally obtained. The numerical solutions were maintained in a pseudo stationary regime. A preliminary study shows that the flows remain laminar throughout the Rayleigh number range considered here.

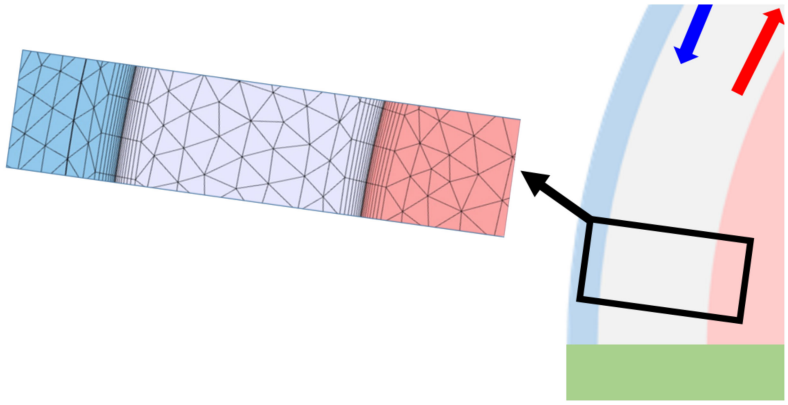

Figure 2. The adopted mesh.

4. Results

The thermal and dynamical characteristics of the flow were determined for all the configurations obtained by combining:

(a) The aspect ratio values A = 0.15, 0.30, 0.50, 0.75, 1.00, 1.25, and 1.5;

(b) The Rayleigh number in the 5.33×10^3–4.50×10^8 range according to the considered values of the heat flux φ and the aspect ratio A as specified in Table 1.

Table 1. Ra_L—A ranges.

A	0.15	0.30	0.50	0.75	1.00	1.25	1.5
Ra_L min	5.33×10^3	8.54×10^4	6.59×10^5	3.33×10^6	1.05×10^7	2.57×10^7	5.33×10^7
Ra_L max	8.20×10^4	1.31×10^6	1.01×10^7	5.13×10^7	1.62×10^8	3.95×10^8	4.50×10^8

Results of a dimensionless temperature field and streamlines Ψ corresponding to the case (A = 0.3; $Ra_L = 1.12 \times 10^6$) are presented in Figure 3.

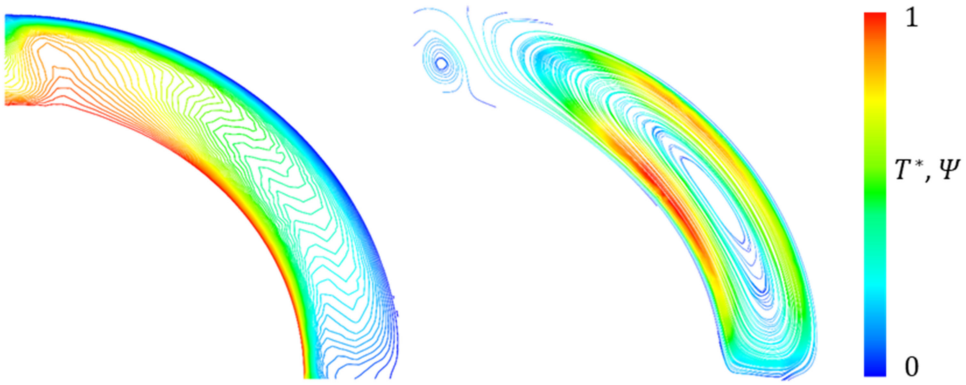

Figure 3. Dimensionless temperature T^* and streamlines Ψ for A = 0.3; $Ra_L = 1.12 \times 10^6$.

The results are consistent with those obtained in conventional closed cavity configurations. They confirm an upward flow on the hot wall side and downward on the cold wall side. This is only an illustration of the flow, the objective of the work being to quantify the convective heat transfer occurring in this cavity.

The ratio between:

(a) The convective power:

$$\oint -\lambda \frac{\partial T}{\partial n} dS \tag{5}$$

where n is the outgoing normal to the surface S; and

(b) The pure conductive power (immobile fluid) exchanged through the air gap between the hot inner wall at temperature $\overline{T}_h$ and the cold outer one at temperature T_c.

$$\frac{\overline{T}_h - T_c}{\left(\frac{1/R_i - 1/R_e}{4\pi\lambda}\right)} \tag{6}$$

allows determination of the average Nusselt number with:

$$\overline{Nu}_L = \frac{-L}{4\pi R_e R_i (\overline{T}_h - T_c)} \oint \frac{\partial T}{\partial n} dS \tag{7}$$

whose value has been calculated for all the considered combinations $(A,\ Ra_L)$ previously specified. Evolution of $\overline{Nu}_L$ versus Ra_L presented in Figure 4a is clearly of the power type:

$$\overline{Nu}_L = k(A) Ra_L^{m(A)} \tag{8}$$

confirmed by its version in the logarithmic co-ordinates presented in Figure 4b for each treated aspect ratio A.

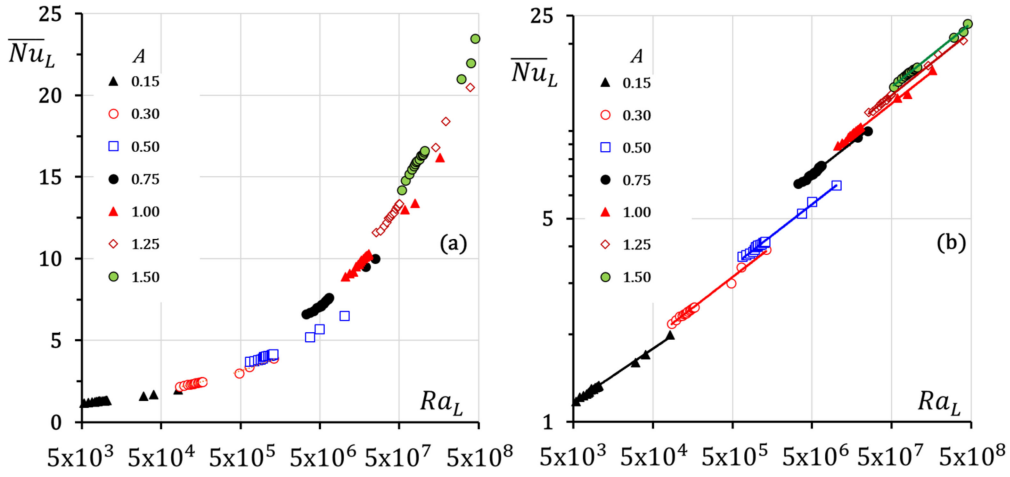

Figure 4. Evolution of $\overline{Nu}_L$ versus Ra_L (**a**) semi-logarithmic co-ordinates; (**b**) logarithmic co-ordinates.

The evolution of the exponent $m(A)$ and coefficient $k(A)$ are presented in Figure 5. This figure shows that the best fits obtained by means of the least square optimization method are of the polynomial type. They are obtained with coefficients of determination higher than 0.998. It is interesting to note that the values of the exponent $m(A)$ vary between 0.185 and 0.223. They remain below 0.25, a characteristic value of natural laminar convective flows in a confined environment. These results also confirm a clear trend towards pure conductive-type flows for low Ra_L values.

The average Nusselt number can, therefore, be calculated with the correlation:

$$\left\{ \begin{array}{c} \overline{Nu}_L = k(A) Ra_L^{m(A)} \\ \text{with} \\ k(A) = -0.0049A^2 + 0.0141A + 0.2481 \\ \text{and} \\ m(A) = -0.0252A^2 + 0.0669A + 0.1759 \\ \text{Valid for } Ra_L - A \text{ ranges specified in Table 1} \end{array} \right\} \tag{9}$$

obtained with a high determination coefficient of 0.995.

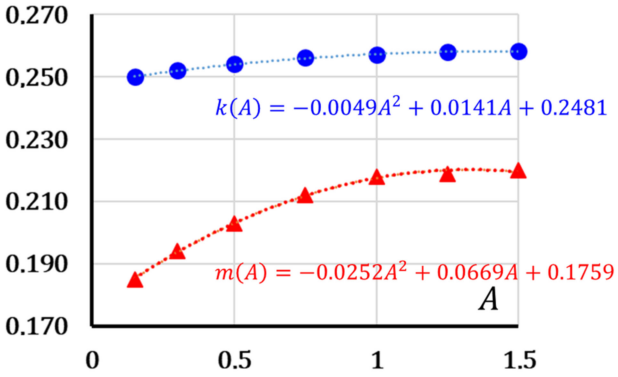

Figure 5. Evolution versus A of the exponent $m(A)$ and coefficient $k(A)$ of Equation (8).

Values calculated by means of Equation (9) denoted as $(\overline{Nu}_L)_{(9)}$ were compared to those determined with the direct simulations $(\overline{Nu}_L)_s$. Deviation $\delta = (\overline{Nu}_L)_s - (\overline{Nu}_L)_{(9)} / (\overline{Nu}_L)_s$ represented in Figure 6 is acceptable, varying between −6.6 and +6.9%, with an average value of +0.8%.

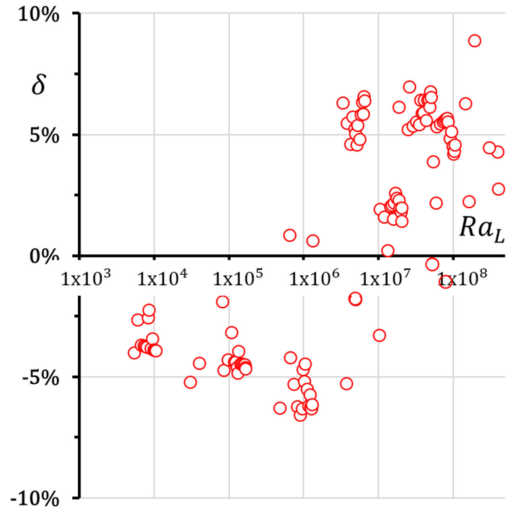

Figure 6. Deviation $\delta = (\overline{Nu}_L)_s - (\overline{Nu}_L)_{(9)} / (\overline{Nu}_L)_s$.

By interpolating these results over the entire Rayleigh number range without taking into account the aspect ratio, the correlation is simplified as follows:

$$\overline{Nu}_L = 0.1 Ra_L^{0.27}$$
$$\text{Valid for } 5.33 \times 10^3 \leq Ra_L \leq 4.50 \times 10^8 \tag{10}$$

with a coefficient of determination of 0.9943. With the average value being +5.1%, it is represented in Figure 7a, accompanied by deviations $\delta' = (\overline{Nu}_L)_s - (\overline{Nu}_L)_{(10)} / (\overline{Nu}_L)_s$ in Figure 7b, ranging between −14.7% and +14.9%.

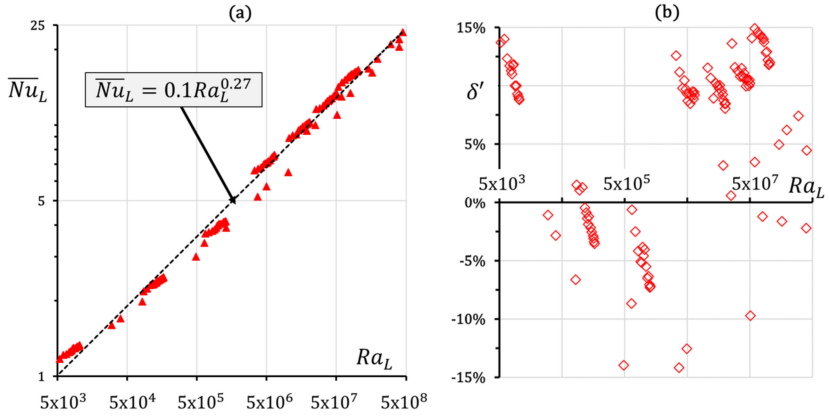

Figure 7. (**a**) Evolution of $\overline{Nu}_L$ versus Ra_L in Equation (10). (**b**) Deviation $\delta' = \left(\overline{Nu}_L\right)_s - \left(\overline{Nu}_L\right)_{(10)} / \left(\overline{Nu}_L\right)_s$.

To the authors' knowledge, there is no work dealing with the geometry discussed here. A comparison is nevertheless made with work quantifying the free convective heat transfer around whole concentric spheres, whose correlations have been adapted to the definitions adopted in the present work. The comparison presented in Figure 8a has been carried out with:

(a) Results of [17] concerning spheres subjected to constant heat flux:

$$\left(\overline{Nu}_L\right)_{(11)} = 0.530Ra^{0.195}$$
$$\text{Valid for } 1.2 \times 10^4 \leq Ra_L \leq 1.0 \times 10^7 \text{ and } A = 1 \tag{11}$$

completed by:

$$\left(\overline{Nu}_L\right)_{(12)} = 1.136Ra_L^{0.091}$$
$$\text{Valid for } 1 \times 10^2 \leq Ra_L \leq 1 \times 10^4;\ Pr = 0.1 \tag{12}$$

for quasi-conductive regimes.

(b) Results of [18]:

$$\left(\overline{Nu}_L\right)_{(13)} = 0.228(A.Ra_L)^{0.226}$$
$$\text{Valid for } 1.2 \times 10^2 \leq A.Ra_L \leq 1.1 \times 10^4;\ 0.09 \leq A \leq 1.81;\ 0.7 \leq Pr \leq 4148 \tag{13}$$

(c) Results of [16]:

$$\left(\overline{Nu}_L\right)_{(14)} = 0.3725A^{0.2187}Ra_L^{0.25} \tag{14}$$

Figure 8b presents the deviations $\delta'' = \left[\left(\overline{Nu}_L\right)_{(R)} - \left(\overline{Nu}_L\right)_s\right] / \left(\overline{Nu}_L\right)_{(R)}$ between the Nusselt number corresponding to any study denoted as $\left(\overline{Nu}_L\right)_{(R)}$ and that of the direct simulations in the present work. For low Rayleigh numbers less than 1×10^4, the average Nusselt number obtained with Equations (13) and (14) is substantially consistent with that of the semi-hemisphere, with a mean deviation of almost zero and 19%, respectively. On the other hand, it is quite far from the results from Equation (11), the average deviation being of about 56%. In the rest of the Rayleigh number range, the Nusselt number is significantly different for both geometries, varying in the 46.5–62.2% and 34.7–42.2% range with Equations (11) and (13), respectively. These results clearly confirm that the thermal and dynamic phenomena are different for the two geometries and that the correlations available in the literature concerning whole spheres cannot reasonably be used for the semi-hemisphere treated in the present work.

5. Conclusions

A numerical approach based on the volume control method using the SIMPLE algorithm was used to quantify the convective exchanges occurring in an open air-filled cavity of semi-hemispherical shape. The results show that the correlations available in the literature dealing with free convective heat transfer around whole spheres cannot be used, given the significant deviations between the Nusselt number concerning the two geometries. The average Nusselt number can be determined in the wide $5.33 \times 10^3 - 4.50 \times 10^8$. Rayleigh number range with the new correlation proposed in this work, which allows its application in electronic packaging. Results also show that the flow remains globally laminar throughout the considered range of the Rayleigh number and for all the considered enclosure's aspect ratios.

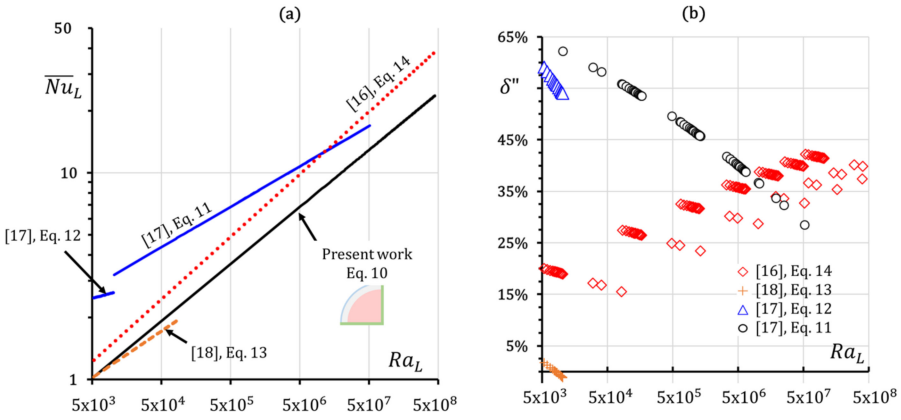

Figure 8. Comparison with other work dealing with whole concentric spheres (**a**) Average Nusselt number (**b**) deviation.

Author Contributions: All authors contributed equally to all the steps of the work and the manuscript. All authors have read and agreed to the published version of the manuscript.

Funding: This research did not receive external funding.

Institutional Review Board Statement: Not applicable.

Informed Consent Statement: Not applicable.

Data Availability Statement: Not applicable.

Conflicts of Interest: The authors declare no conflict of interest.

Nomenclature

A	enclosure aspect ratio (-)
a	air thermal diffusivity (m^2s^{-1})
C_p	air specific heat ($J{\cdot}kg^{-1}K^{-1}$)
$\vec{e}_g$	vector opposite to the gravity field
g	acceleration of the gravity ($m{\cdot}s^{-2}$)
k	coefficient in Equation (8)
L	distance between the cold and hot walls (m)
m	exponent in Equation (8)
n	outgoing normal
$\overline{Nu}_L$	mean Nusselt number (-)
p	pressure (Pa)
p^*	dimensionless pressure (-)
Pr	Prandtl number (-)
R_e	radius of the external semi-hemisphere (m)

R_i	radius of the internal semi-hemisphere (m)
Ra_L	Rayleigh number (-)
S	surface (m^2)
T	temperature (K)
T_c	external semi-hemisphere mean temperature (K)
$\overline{T}_h$	internal semi-hemisphere mean temperature (K)
T^*	dimensionless temperature (-)
$\vec{u}$	velocity vector
$\vec{u}^*$	dimensionless velocity vector (-)
Greek symbols	
β	air volumetric coefficient of expansion (K^{-1})
δ	$\delta = \left(\overline{Nu}_L\right)_s - \left(\overline{Nu}_L\right)_{(9)} / \left(\overline{Nu}_L\right)_s$ deviation (%)
δ'	$\delta' = \left(\overline{Nu}_L\right)_s - \left(\overline{Nu}_L\right)_{(10)} / \left(\overline{Nu}_L\right)_s$deviation(%)
δ''	$\delta'' = \left[\left(\overline{Nu}_L\right)_{(R)} - \left(\overline{Nu}_L\right)_s\right] / \left(\overline{Nu}_L\right)_{(R)}$ deviation (%)
∇^{*2}	operator Laplacian
$\vec{\nabla}^*$	operator nabla
φ	heat flux (Wm^{-2})
λ	thermal conductivity of air (W/mK)
μ	dynamic viscosity of air (Pa·s)
ρ	density of air ($kg \cdot m^{-3}$)
Ψ	streamlines
Subscripts	
(9)–(14)	from Equation (9) to Equation (14)
(R)	from any reference
s	from direct simulation

References

1. Basak, T.; Anandalakshmi, R.; Biswal, T. Analysis of convective heat flow visualization within porous right angled triangular enclosures with a concave/convex hypotenuse. *Numer. Heat Transf. Part A Appl.* **2013**, *64*, 621–647. [CrossRef]
2. Sheremet, M.A.; Grosan, T.; Pop, I. Thermal convection in a chamber filled with a nanosuspension driven by a chemical reaction using Tiwari and Das' model. *Int. J. Numer. Methods Heat Fluid Flow* **2020**, in press. [CrossRef]
3. Baudoin, A.; Saury, D.; Zhu, B.; Boström, C. Experimental optimization of passive cooling of a heat source array flush-mounted on a vertical plate. *Energies* **2016**, *9*, 912. [CrossRef]
4. Oztop, H.F.; Almeshaal, M.A.; Kolsi, L.; Rashidi, M.M.; Ali, M.E. Natural convection and irreversibility evaluation in a cubic cavity with partial opening in both top and bottom sides. *Entropy* **2019**, *21*, 116. [CrossRef] [PubMed]
5. Baïri, A. Transient thermal characteristics of airborne electronic equip-ment with discrete hot bands in a confined environment. *Appl. Energy* **2008**, *85*, 951–967. [CrossRef]
6. IMiroshnichenko, V.; Sheremet, M.A.; Mohamad, A.A. The influence of surface radiation on the passive cooling of a heat-generating element. *Energies* **2019**, *12*, 980. [CrossRef]
7. Shiina, Y.; Fujimura, K.; Kunugi, T.; Akino, N. Natural convection in hemispherical enclosure heated from below. *Int. J. Heat Mass Transf.* **1994**, *37*, 1605–1617. [CrossRef]
8. Baïri, A. A synthesis of correlations on quantification of free convective heat transfer in inclined air-filled hemispherical enclosures. *Int. Commun. Heat Mass Transf.* **2014**, *59*, 174–177. [CrossRef]
9. Abu-Nada, E. Modeling of various heat transfer problems using dissipative particle dynamics. *Numer. Heat Transf. Part A Appl.* **2010**, *58*, 660–679. [CrossRef]
10. Haddad, O.; Baïri, A.; Alilat, N.; Bauzin, J.G.; Laraqi, N. Free convec-tion in ZnO nanofluid-filled and tilted hemispherical enclosures containing a cubic electronic device. *Int. Commun. Heat Mass Transf.* **2017**, *87*, 204–211. [CrossRef]
11. Baïri, A.; Haddad, O.; Alilat, N. Nu-Ra-Pr correlations for nanofluidic natural convection in tilted hemispherical enclosures with active disk. *Numer. Heat Transf.* **2017**, *71*, 1094–1103. [CrossRef]
12. Alilat, N. Natural convective heat transfer in the air-filled interstice be-tween inclined concentric hemispheres: Application to thermoregulation in electronics. *Int. J. Numer. Methods Heat Fluid Flow* **2017**, *27*, 2375–2384. [CrossRef]
13. Alilat, N.; Haddad, O.; Baïri, A. Numerical study of natural convection of ZnO-water nanofluid enclosed between two inclined and concentric hemispheres. *Eur. Phys. J. Plus* **2020**, *135*, 146–163. [CrossRef]
14. Baïri, A.; Laraqi, N. Experimental quantification of natural convective heat transfer within annulus space filled with a H_2O-Cu nanofluid saturated porous medium. Application to electronics cooling. *Exp. Heat Transf.* **2019**, *32*, 364–375. [CrossRef]
15. Sheremet, M.A. Mathematical simulation of unsteady natural convection inside a sphere. *Comput. Therm. Sci. Int. J.* **2011**, *3*, 277–287. [CrossRef]

16. Raithby, G.; Hollands, K. A general method of obtaining approximate solutions to laminar and turbulent free convection problems. *Adv. Heat Transf.* **1975**, *11*, 265–315.
17. Tazi-Charki, M.N.; Daoudi, S.; le Palec, G.; Daguenet, M. Etude numérique du modèle de Boussinesq de convection naturelle laminaire axisymétrique permanente dans un espace annulaire compris entre deux sphères. *Rev. Générale Therm.* **1997**, *36*, 239–251. [CrossRef]
18. Scanlan, J.A.; Bishop, E.H.; Powe, R.E. Natural convection heat transfer between concentric spheres. *Int. J. Heat Mass Transf.* **1970**, *13*, 1859–1872. [CrossRef]
19. Teertstra, P.; Yovanovich, M.; Culham, J.R. Natural convection meas-urements for a concentric spherical enclosure. *J. Heat Transf.* **2006**, *128*, 580–587. [CrossRef]
20. Garg, V.K. Natural convection between concentric spheres. *Int. J. Heat Mass Transf.* **1992**, *35*, 1935–1945. [CrossRef]
21. Baïri, A.; Martín-Garín, A.; Alilat, N.; Roseiro, L.; Millán-García, J.A. Quantification of free convection in a quarter-spherical innovative Trombe wall design. *J. Build. Eng.* **2021**, *42*, 102443. [CrossRef]
22. Pastori, S.; Mereu, R.; Mazzucchelli, E.S.; Passoni, S.; Dotelli, G. Energy performance evaluation of a ventilated façade system through CFD modeling and comparison with international standards. *Energies* **2021**, *14*, 193. [CrossRef]
23. Baïri, A.; Martín-Garín, A.; Ilinca, A.; Alilat, N.; Millán-García, J.A. Thermal state of a concentric quarter spherical enclosure subjected to air free convection. *J. Therm. Anal. Calorim.* **2021**. [CrossRef]
24. Bejan, A. *Convection Heat Transfer*, 4th ed.; John Wiley & Sons, Inc.: Hoboken, NJ, USA, 2013. [CrossRef]